Generation of Two-Dimensional Structured Meshes for Simply and Doubly Connected Regions

Agatha Penteado de Almeida
Federal University of Technology – Paraná

Rudimar Luiz Nós
Federal University of Technology – Paraná

We present in this work Thompson's equations, with spacing factors P and Q, and we use them to computationally generate two-dimensional structured meshes for simply and doubly connected regions. For the internal boundary of doubly connected regions we selected some wing profiles of an aircraft. We discretized the equations using second-order centered finite differences and we used the SOR method to numerically solve the system of linear equations resulting from discretization. In SOR method, we test optimal values for the relaxation parameter ω. We conclude that the combination of SOR and finite difference methods produced adequate meshes for certain wing profiles and values of P, Q, and ω.

Keywords: Thompson's equations, structured meshes, wing profiles of an aircraft, SOR method

INTRODUCTION

Partial Differential Equations (PDEs) define several mathematical models used to simulate physical phenomena (Figueiredo, 1997; Figueiredo; Neves, 1997; Fortuna, 2000; Iório, 1989), such as models in fluid dynamics and aerodynamics. In the latter, computer simulations have significantly reduced the time and costs to produce an aircraft.

To numerically simulate the mathematical model that describes a physical phenomenon, we must first discretize the spatial domain. To do so, we can employ structured meshes or unstructured meshes. In two dimensions, structured meshes are formed by four-sided cells, while in three dimensions, by six-sided volumetric cells (hexahedral cells), as illustrated in Figure 1. In these meshes, each computational cell has the same number of neighboring cells, and, in two dimensions, the nodes of each cell are identified by the indexes i and j.

FIGURE 1
STRUCTURED MESHES: (A) TWO-DIMENSIONAL RADIAL; (B) THREE-DIMENSIONAL

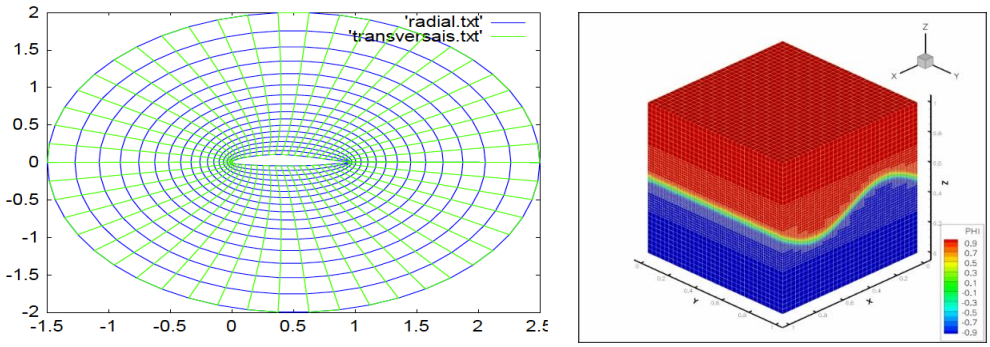

(a) (b)

Source: (a) Almeida (1997); (b) Nós (2007).

Structured and unstructured meshes can be used for simply or multiply connected regions (or domains). A region R is simply connected when any closed curve contained in it can be reduced to a point. When this is not possible, the region is multiply connected (Polina et al., 1989). Figure 2 illustrates simply and doubly connected regions. In a simply connected domain there is no internal boundary; in a doubly connected one, there is an internal boundary.

FIGURE 2
MESH STRUCTURED DOMAIN: (A) SIMPLY CONNECTED; (B) DOUBLY CONNECTED

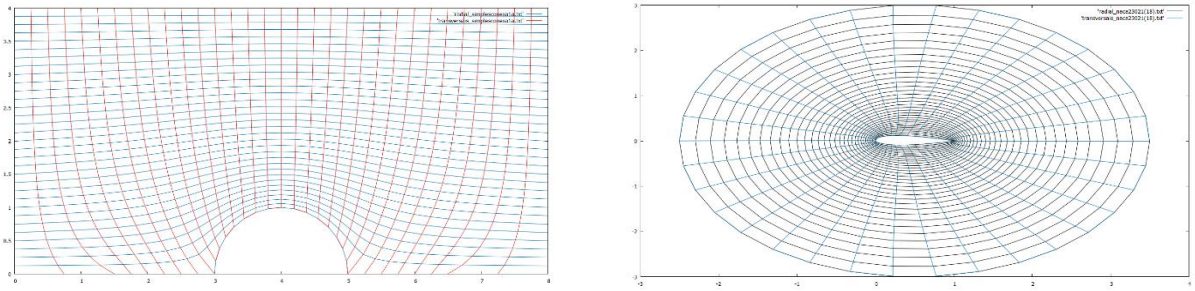

(a) (b)

Source: Almeida (1997).

In this work, we employ the Thompson equations (THOMPSON, 1985) to computationally generate two-dimensional structured meshes for single and doubly connected regions. We discretize these equations using the finite difference method (Fortuna, 2000) and solve the linear system arising from the discretization by means of the successive over-relaxation (SOR) method (Burden; Faires, 1997), with optimized relaxation parameter ω. We built computational codes in C language (Almeida, 2017, 2018) compiled and executed in *Dev-C++* (Bloodshed, 2022), and visualized the generated meshes in *gnuplot 5.0 patchlevel 3* (Gnuplot, 2022). We also employed *Adobe Illustrator CC 2015* (Adobe, 2022) to construct some figures. All computational simulations were run on a *MacBook Pro* (13-inch, Mid 2012) with a 2.5 GHz Intel Core i5 processor and 8GB RAM.

For simply connected domains, we chose as boundary the arc and the diffuser; for doubly connected domains, we selected as internal boundary some airfoil (aircraft wing) profiles of the NACA type (AIRFOILTOOLS, 2022; UIUC, 2022).

According to Suckow (2009), although the Wright Brothers made the first flight in 1903, the United States of America was, during World War I, behind Europe in air technology. To reverse this situation, the U.S. Congress founded, on March 3, 1915, the National Advisory Committee for Aeronautics (NACA).

The 4-digit NACA airfoils were the first family of airfoils designed using analytical equations that describe the camber (curvature) of the midline (geometric centerline) of the airfoil and the thickness distribution along that line (Stanford, n.d.). The first digit specifies the maximum camber (bulge) in percent of the chord (airfoil length); the second digit indicates the position of the maximum camber along the chord, in tenths of the chord; the last two digits give the maximum thickness in percent of the chord. The camber is the distance, perpendicular to the chord, between the chord and the midline, as illustrated in Figure 3.

FIGURE 3
MAIN ELEMENTS OF AN AIRCRAFT'S AIRFOIL

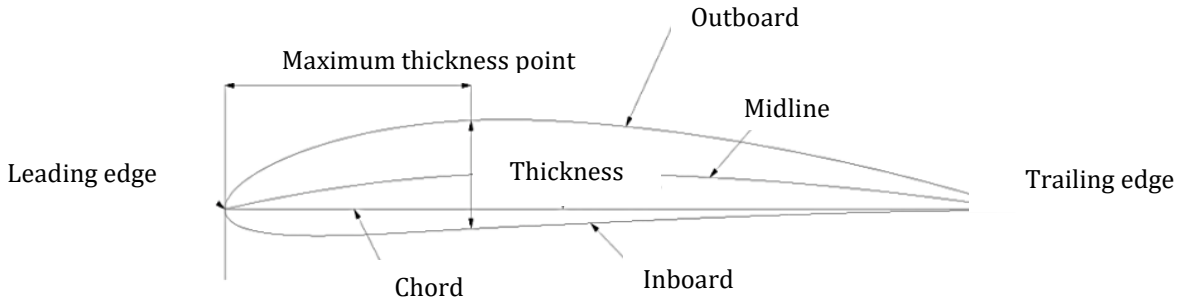

Source: Google (2017).

For example, NACA0006 has a 0% bulge, maximum distance to the centerline occurring at 0.0 of the chord, and a thickness of 6% of the chord length. Figure 4 illustrates two 4-digit NACA profiles.

The 5-digit NACA airfoils use the same thickness format as the 4-digit ones, but the midline is defined differently, and the nomenclature is a bit more complex. The first digit, when multiplied by 1.5, gives the design lift coefficient, which means that the airfoil is designed for a given lift coefficient in tenths of the chord; the next two digits, when divided by 2, give the maximum camber position in tenths of the chord; the last two digits again give the maximum thickness in percent of the chord. As an example, NACA23021 has a lift coefficient of 0.3, a maximum camber located 15% from the leading edge, and a maximum thickness of 21%. Two 5-digit NACA profiles are illustrated in Figure 5.

FIGURE 4
AIRFOIL PROFILES: (A) NACA0006; (B) NACA2408

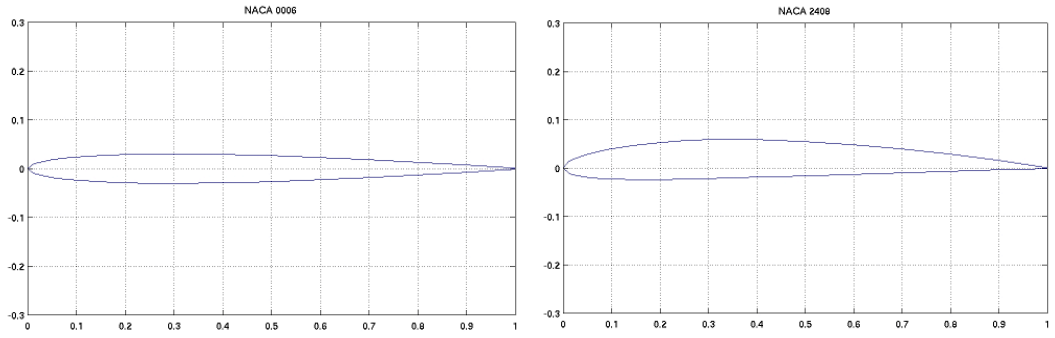

(a) (b)

Source: UIUC (2022).

FIGURE 5
AIRFOIL PROFILES: (A) NACA23021; (B) NACA25112

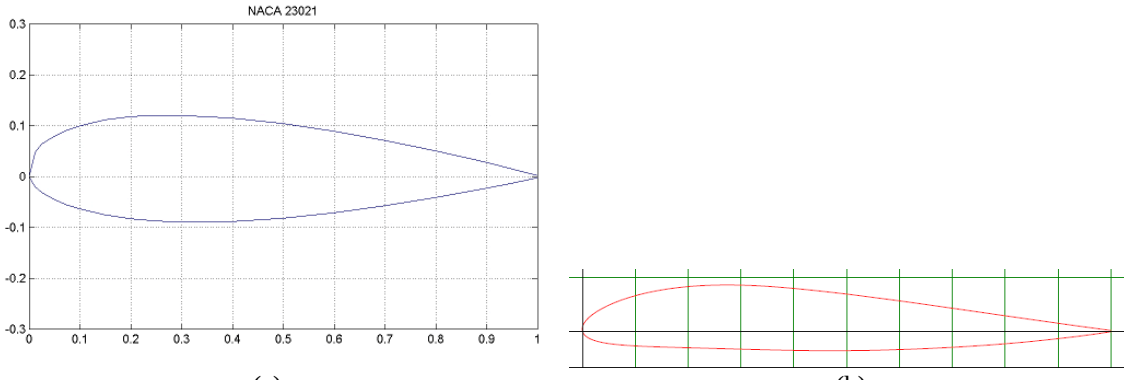

(a) (b)

Source: (a) UIUC (2022); (b) Airfoiltools (2022).

On NACA 7-series airfoils, the first digit indicates the 7-series; the second digit, the minimum outboard pressure position, in tenths of the chord; the third digit, the minimum inboard pressure position, in tenths of the chord; the letter in the fourth digit indicates the thickness distribution and mean curvature line shapes used; the fifth digit is the design lift coefficient, in tenths of the chord; the last two digits indicate the maximum airfoil thickness, in percent of the chord. For example, the NACA747A415 is 7-series, the minimum pressure position on the extrados is 0.4 of the chord, the minimum pressure position on the intrados is 0.7 of the chord, the thickness distribution and mean curvature line shapes used are Type A, the design lift coefficient is 0.4 of the chord, and the maximum airfoil thickness is 15%. A NACA 7-series profile is illustrated in Figure 6.

FIGURE 6
NACA747A415 PROFILE

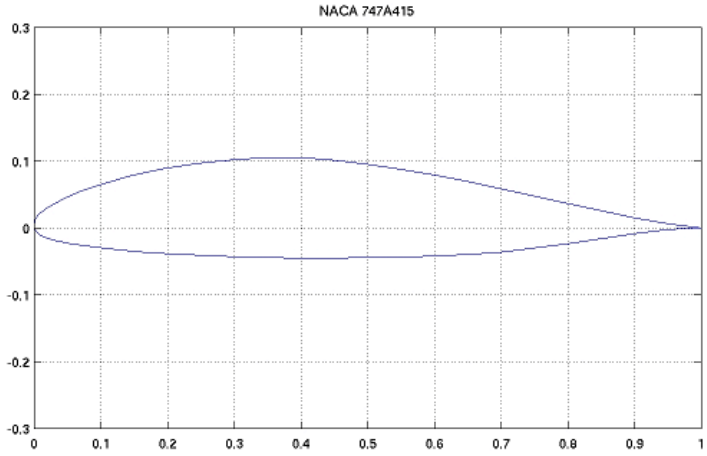

Source: UIUC (2022).

THE MATHEMATICAL MODEL

Thompson's equations:

$$\alpha \frac{\partial^2 x}{\partial \xi^2} - 2\beta \frac{\partial^2 x}{\partial \xi \partial \eta} + \gamma \frac{\partial^2 x}{\partial \eta^2} + J^2 \left(P \frac{\partial x}{\partial \xi} + Q \frac{\partial x}{\partial \eta} \right) = 0, \tag{1}$$

$$\alpha \frac{\partial^2 y}{\partial \xi^2} - 2\beta \frac{\partial^2 y}{\partial \xi \partial \eta} + \gamma \frac{\partial^2 y}{\partial \eta^2} + J^2 \left(P \frac{\partial y}{\partial \xi} + Q \frac{\partial y}{\partial \eta} \right) = 0, \tag{2}$$

with

$$\alpha = \left(\frac{\partial x}{\partial \eta} \right)^2 + \left(\frac{\partial y}{\partial \eta} \right)^2, \tag{3}$$

$$\beta = \frac{\partial x}{\partial \xi} \frac{\partial x}{\partial \eta} + \frac{\partial y}{\partial \xi} \frac{\partial y}{\partial \eta}, \tag{4}$$

$$\gamma = \left(\frac{\partial x}{\partial \xi} \right)^2 + \left(\frac{\partial y}{\partial \xi} \right)^2, \tag{5}$$

$$J = \frac{\partial x}{\partial \xi} \frac{\partial y}{\partial \eta} - \frac{\partial x}{\partial \eta} \frac{\partial y}{\partial \xi}, \tag{6}$$

are obtained from conformal transformations on the two-dimensional Laplace equation (Thompson, 1985). These equations constitute a system of nonlinear, second order, homogeneous PDEs. In equations (1)-(6), (x, y) are Cartesian coordinates, (ξ, η) are generalized coordinates (in these, lines from the same family do not intersect, while lines from distinct families intersect only once) and $P(x, y)$ and $Q(x, y)$ are functions that control the mesh spacing, i.e., these functions enable the concentration of the coordinate lines in the desired regions (Polina et al., 1989). In this work, we adopt $P, Q \in \mathbb{R}$, that is, P and Q are real constants.

THE DISCRETE MODEL

Employing second-order centered finite differences (Fortuna, 2000), we write the Thompson equations with spacing factors (1)-(6) in discrete form as:

$$\alpha_{i,j} \frac{x_{i+1,j} - 2x_{i,j} + x_{i-1,j}}{(\Delta\xi)^2} - 2\beta_{i,j} \frac{x_{i+1,j+1} - x_{i+1,j-1} - x_{i-1,j+1} + x_{i-1,j-1}}{4\Delta\xi\Delta\eta} +$$
$$+\gamma_{i,j} \frac{x_{i,j+1} - 2x_{i,j} + x_{i,j-1}}{(\Delta\eta)^2} + {J_{i,j}}^2 \left(P \frac{x_{i+1,j} - x_{i-1,j}}{2\Delta\xi} + Q \frac{x_{i,j+1} - x_{i,j-1}}{2\Delta\eta} \right) = 0; \tag{7}$$

$$\alpha_{i,j} \frac{y_{i+1,j} - 2y_{i,j} + y_{i-1,j}}{(\Delta\xi)^2} - 2\beta_{i,j} \frac{y_{i+1,j+1} - y_{i+1,j-1} - y_{i-1,j+1} + y_{i-1,j-1}}{4\Delta\xi\Delta\eta} +$$
$$+\gamma_{i,j} \frac{y_{i,j+1} - 2y_{i,j} + y_{i,j-1}}{(\Delta\eta)^2} + {J_{i,j}}^2 \left(P \frac{y_{i+1,j} - y_{i-1,j}}{2\Delta\xi} + Q \frac{y_{i,j+1} - y_{i,j-1}}{2\Delta\eta} \right) = 0, \tag{8}$$

being

$$\alpha_{i,j} = \frac{x_{i,j+1} - x_{i,j-1}}{2\Delta\eta} \frac{x_{i,j+1} - x_{i,j-1}}{2\Delta\eta} + \frac{y_{i,j+1} - y_{i,j-1}}{2\Delta\eta} \frac{y_{i,j+1} - y_{i,j-1}}{2\Delta\eta}, \tag{9}$$

$$\beta_{i,j} = \frac{x_{i+1,j} - x_{i-1,j}}{2\Delta\xi} \frac{x_{i,j+1} - x_{i,j-1}}{2\Delta\eta} + \frac{y_{i+1,j} - y_{i-1,j}}{2\Delta\xi} \frac{y_{i,j+1} - y_{i,j-1}}{2\Delta\eta}, \tag{10}$$

$$\gamma_{i,j} = \frac{x_{i+1,j} - x_{i-1,j}}{2\Delta\xi} \frac{x_{i+1,j} - x_{i-1,j}}{2\Delta\xi} + \frac{y_{i+1,j} - y_{i-1,j}}{2\Delta\xi} \frac{y_{i+1,j} - y_{i-1,j}}{2\Delta\xi}, \tag{11}$$

$$J_{i,j} = \frac{x_{i+1,j}-x_{i-1,j}}{2\Delta\xi}\frac{y_{i,j+1}-y_{i,j-1}}{2\Delta\eta} - \frac{x_{i,j+1}-x_{i,j-1}}{2\Delta\eta}\frac{y_{i+1,j}-y_{i-1,j}}{2\Delta\xi}. \quad (12)$$

The discrete Thompson equations (7)-(12) define a linear system. To solve this system by the SOR method (BURDEN; FAIRES, 1997), we must calculate the residuals rx and ry with respect to variables x and y, respectively. Considering $\Delta\xi = \Delta\eta = 1$ in equations (7)-(12) and k the iteration, as the system is homogeneous, we have that:

$$\begin{aligned} rx_{i,j}{}^{(k)} = {} & \alpha_{i,j}{}^{(k)}\left(x_{i+1,j}{}^{(k-1)} - 2x_{i,j}{}^{(k-1)} + x_{i-1,j}{}^{(k)}\right) + \\ & -\frac{\beta_{i,j}{}^{(k)}}{2}\left(x_{i+1,j+1}{}^{(k-1)} - x_{i+1,j-1}{}^{(k)} - x_{i-1,j+1}{}^{(k-1)} + x_{i-1,j-1}{}^{(k)}\right) + \\ & +\gamma_{i,j}{}^{(k)}\left(x_{i,j+1}{}^{(k-1)} - 2x_{i,j}{}^{(k-1)} + x_{i,j-1}{}^{(k)}\right) + \\ & +\frac{J_{i,j}{}^{(k)}J_{i,j}{}^{(k)}}{2}\left[P\left(x_{i+1,j}{}^{(k-1)} + x_{i-1,j}{}^{(k)}\right) + Q\left(x_{i,j+1}{}^{(k-1)} - x_{i,j-1}{}^{(k)}\right)\right]; \end{aligned} \quad (13)$$

$$\begin{aligned} ry_{i,j}{}^{(k)} = {} & \alpha_{i,j}{}^{(k)}\left(y_{i+1,j}{}^{(k-1)} - 2y_{i,j}{}^{(k-1)} + y_{i-1,j}{}^{(k)}\right) + \\ & -\frac{\beta_{i,j}{}^{(k)}}{2}\left(y_{i+1,j+1}{}^{(k-1)} - y_{i+1,j-1}{}^{(k)} - y_{i-1,j+1}{}^{(k-1)} + y_{i-1,j-1}{}^{(k)}\right) + \\ & +\gamma_{i,j}{}^{(k)}\left(y_{i,j+1}{}^{(k-1)} - 2y_{i,j}{}^{(k-1)} + y_{i,j-1}{}^{(k)}\right) + \\ & +\frac{J_{i,j}{}^{(k)}J_{i,j}{}^{(k)}}{2}\left[P\left(y_{i+1,j}{}^{(k-1)} + y_{i-1,j}{}^{(k)}\right) + Q\left(y_{i,j+1}{}^{(k-1)} - y_{i,j-1}{}^{(k)}\right)\right], \end{aligned} \quad (14)$$

with

$$\begin{aligned} \alpha_{i,j}{}^{(k)} = {} & \frac{1}{4}\left[\left(x_{i,j+1}{}^{(k-1)} - x_{i,j-1}{}^{(k)}\right)\left(x_{i,j+1}{}^{(k-1)} - x_{i,j-1}{}^{(k)}\right)\right. \\ & \left. + \left(y_{i,j+1}{}^{(k-1)} - y_{i,j-1}{}^{(k)}\right)\left(y_{i,j+1}{}^{(k-1)} - y_{i,j-1}{}^{(k)}\right)\right], \\ \beta_{i,j}{}^{(k)} = {} & \frac{1}{4}\left[\left(x_{i+1,j}{}^{(k-1)} - x_{i-1,j}{}^{(k)}\right)\left(x_{i,j+1}{}^{(k-1)} - x_{i,j-1}{}^{(k)}\right)\right. \\ & \left. + \left(y_{i+1,j}{}^{(k-1)} - y_{i-1,j}{}^{(k)}\right)\left(y_{i,j+1}{}^{(k-1)} - y_{i,j-1}{}^{(k)}\right)\right], \\ \gamma_{i,j}{}^{(k)} = {} & \frac{1}{4}\left[\left(x_{i+1,j}{}^{(k-1)} - x_{i-1,j}{}^{(k)}\right)\left(x_{i+1,j}{}^{(k-1)} - x_{i-1,j}{}^{(k)}\right)\right. \\ & \left. + \left(y_{i+1,j}{}^{(k-1)} - y_{i-1,j}{}^{(k)}\right)\left(y_{i+1,j}{}^{(k-1)} - y_{i-1,j}{}^{(k)}\right)\right], \\ J_{i,j}{}^{(k)} = {} & \frac{1}{4}\left[\left(x_{i+1}{}^{(k-1)} - x_{i-1,j}{}^{(k)}\right)\left(y_{i,j+1}{}^{(k-1)} - y_{i,j-1}{}^{(k)}\right)\right. \\ & \left. - \left(x_{i,j+1}{}^{(k-1)} - x_{i,j-1}{}^{(k)}\right)\left(y_{i+1,j}{}^{(k-1)} - y_{i,-1,j}{}^{(k)}\right)\right]. \end{aligned}$$

With the calculated residuals in (13) and (14), the values of x and y are updated by means of the following relations:

$$x_{i,j}{}^{(k)} = x_{i,j}{}^{(k-1)} + \frac{\omega}{2\left(\alpha_{i,j}{}^{(k)} + \gamma_{i,j}{}^{(k)}\right)} rx_{i,j}{}^{(k)}; \quad (15)$$

$$y_{i,j}{}^{(k)} = y_{i,j}{}^{(k-1)} + \frac{\omega}{2\left(\alpha_{i,j}{}^{(k)} + \gamma_{i,j}{}^{(k)}\right)} ry_{i,j}{}^{(k)}. \quad (16)$$

The iterative process defined by equations (13)-(16) is stopped when the set precision ε is reached or when a maximum number of *itmax* iterations is reached. For defining precision, we adopt $\max\left\{rx_{i,j}{}^{(k)}, ry_{i,j}{}^{(k)}\right\} \leq \varepsilon = 10^{-5}$, and for the maximum number of iterations, $itmax = 2000$.

INITIAL AND BOUNDARY CONDITIONS

The boundaries for the diffuser and the arc, the selected simply connected domains, are as defined in Figure 7.

FIGURE 7
SIMPLY CONNECTED DOMAIN BOUNDARIES: (A) DIFFUSER; (B) ARC

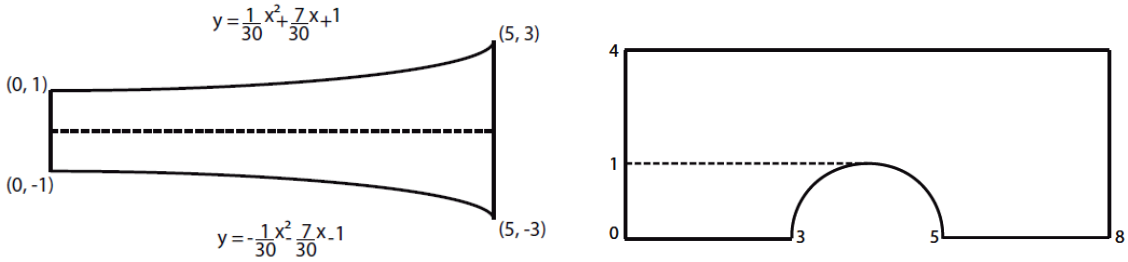

(a) (b)

Source: Almeida (1997).

For the doubly connected regions chosen, we need to define the inner and outer boundaries. As internal boundary we use some points of a NACA, and as external boundary a circle with radius R equal to m times the chord of the airfoil, of measure 1 (we used in the simulations $m = 2, m = 3, m = 4.5$ and $m = 8$). Thus, the mesh for the doubly connected region will have radial and transverse lines. In rectangular coordinates, a cut line defines the vertical boundaries; the NACA points, the lower horizontal boundary; the circle of radius $R = m$, the upper horizontal boundary. The remaining vertical lines are the transversals, while the remaining horizontal lines are the radials, as illustrated in Figure 8.

FIGURE 8
GEOMETRY FOR THE NACA

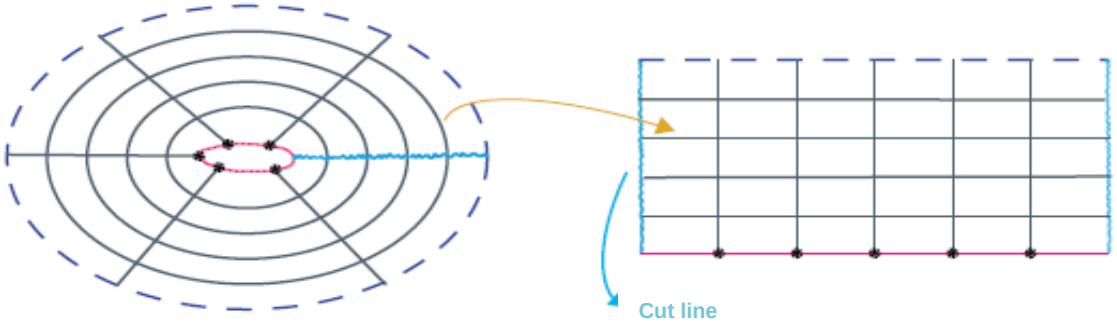

Source: Almeida (1997).

In the process of calculating $x_{i,j}$ and $y_{i,j}$, the horizontal boundaries are kept unchanged while the vertical boundaries are updated at each step of the iterative process. Thus, $i = 0,1, \dots, i_{max}$ and $j = 1, \dots, j_{max} - 1$. Once we determine the values $x_{i_{max},j}$ and $y_{i_{max},j}$ on the right vertical boundary, we impose these values on the corresponding $x_{0,j}$ and $y_{0,j}$ values on the left vertical boundary. In this way, the vertical boundaries remain with the same values, i.e., $x_{0,j} = x_{i_{max},j}$ and $y_{0,j} = y_{i_{max},j}$, $j = 1, \dots, j_{max} - 1$. However, to compute the values $x_{i_{max},j}$ and $y_{i_{max},j}$, we need the "ghost values" $x_{i_{max}+1,j}$ and $y_{i_{max}+1,j}$. Since we do not have these values, we impose that $x_{i_{max}+1,j} = x_{1,j}$ and $y_{i_{max}+1,j} = y_{1,j}, j = 1, \dots, j_{max} -$

1. This strategy, illustrated in Figure 9, is equivalent to adopting periodic boundary conditions in the horizontal direction.

As for the initial conditions, the internal points of the mesh are initially determined by transfinite interpolation of the boundary conditions. Transfinite interpolation is a form of two-dimensional linear interpolation (Almeida, 2017; Paiva, 2013). In the doubly connected region, the cut-off line points are initiated considering a linear distribution for the abscissae and zero for the ordinates.

FIGURE 9
GHOST POINTS IN THE DOUBLY CONNECTED DOMAIN

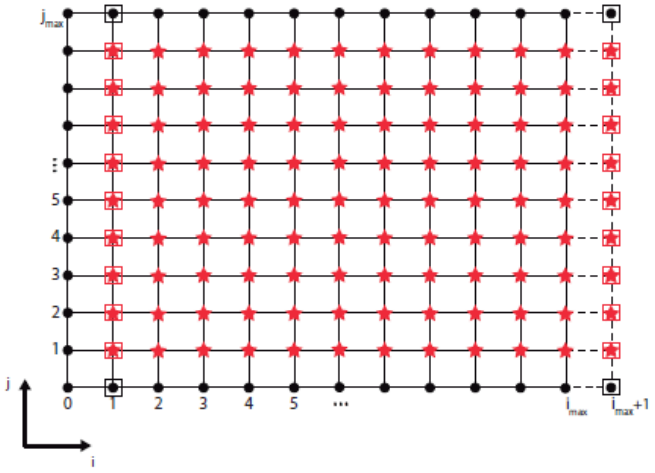

Source: Almeida (1997).

COMPUTER SIMULATIONS

Optimal Value for the Relaxation Parameter ω in the SOR Method

We selected two geometries, the arc (simply connected domain) and NACA0006 (doubly connected domain), to test optimal values for the relaxation parameter ω in the SOR method. Tables 1 and 2 list the results of these tests.

TABLE 1
CONVERGENCE OF THE SOR METHOD FOR SIMPLY CONNECTED DOMAIN (ARC) WITH $P = Q = 0$

ω	1.0	1.1	1.2	1.3	1.4	1.5	1.6	1.7	1.8	1.9	2.0
Iterations	549	457	380	314	256	205	158	110	109	2000	1397
Convergence	yes	yes	yes	yes	yes	yes	yes	yes	yes	no	yes

Source: Almeida (1997).

TABLE 2
CONVERGENCE OF THE SOR METHOD FOR DOUBLY CONNECTED DOMAIN (NACA0006) WITH $P = Q = 0$ AND $R = 2$

ω	1.0	1.1	1.2	1.3	1.4	1.5	1.6	1.7	1.8	1.9
iterations	2000	2000	2000	2000	2000	156	121	1019	1215	2000
convergence	No	no	no	no	no	yes	yes	no	no	no

Source: Almeida (1997).

Diffuser

The diffuser is a structure used to slow down a flow with as little total pressure loss as possible. Figures 10 and 11 illustrate the computationally generated meshes from the geometry described in Figure 7(a).

FIGURE 10
MESH FOR THE DIFFUSER WITH $P = Q = 0$, $\omega = 1.8$ AND 79 ITERATIONS WITH THE SOR METHOD

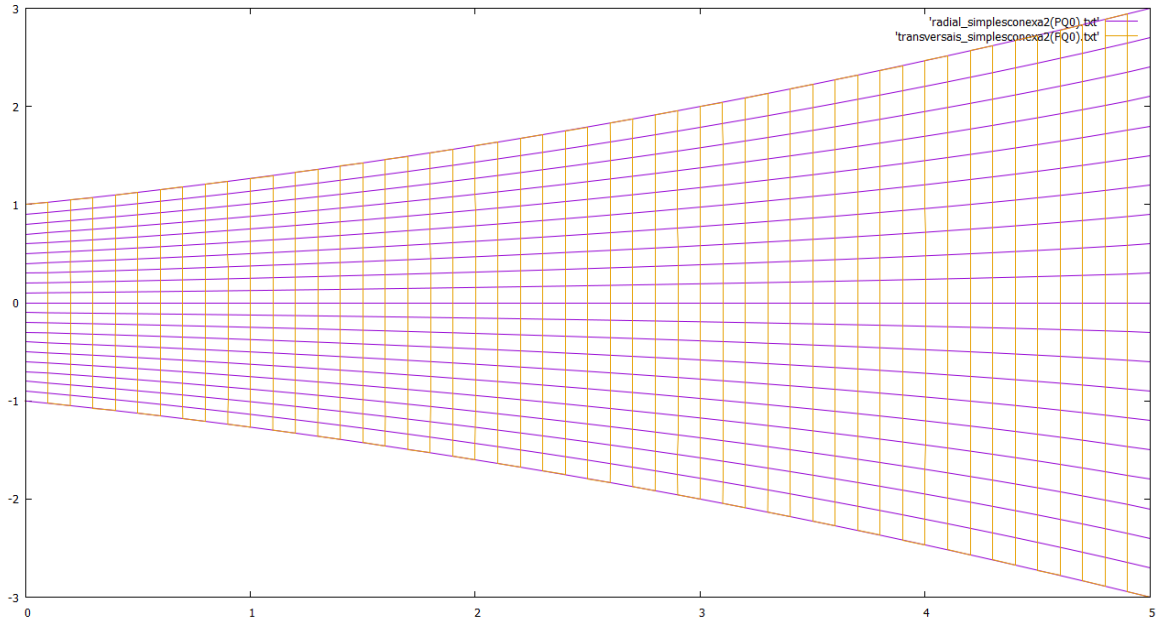

Source: Almeida (1997).

FIGURE 11
MESH FOR THE DIFFUSER WITH $P = -2$ AND $Q = 2$, $\omega = 1.8$ AND 83 ITERATIONS WITH THE SOR METHOD

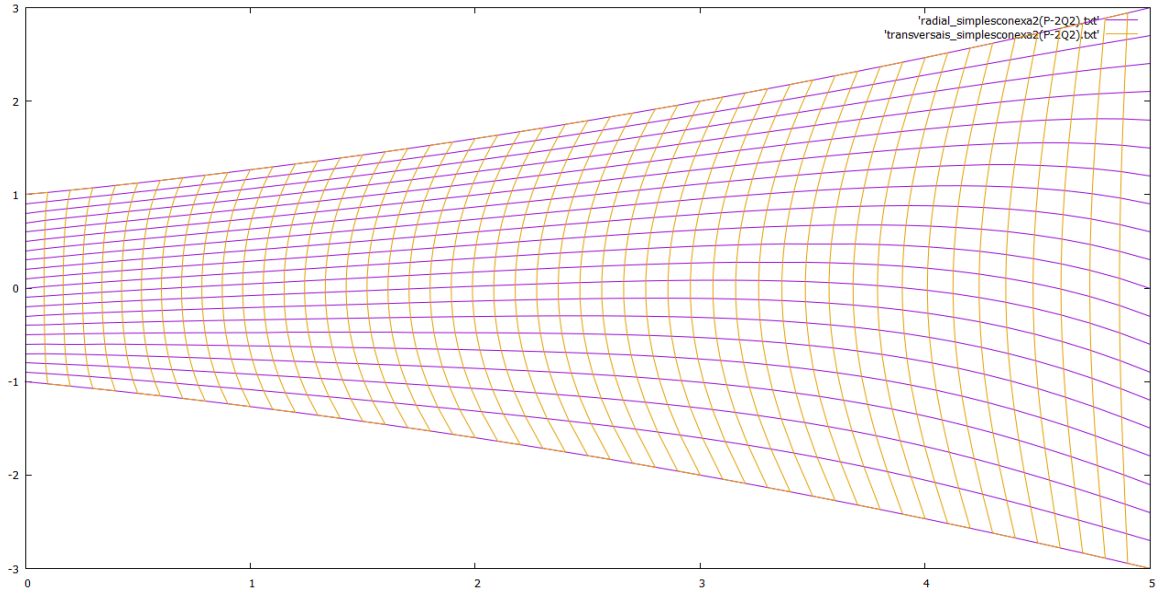

Source: Almeida (1997).

Arc

Figures 12 and 13 illustrate the meshes computationally generated from the geometry described in Figure 7(b).

FIGURE 12
MESH FOR THE ARC WITH $P = Q = 0$, $\omega = 1.8$ AND 109 ITERATIONS WITH THE SOR METHOD

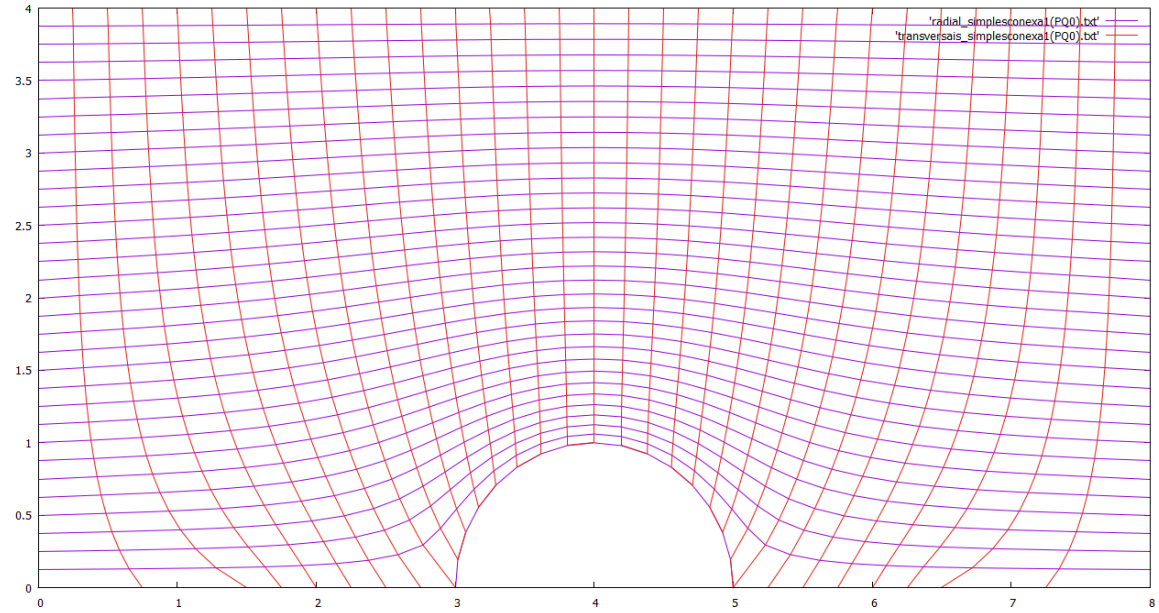

Source: Almeida (1997).

FIGURE 13
MESH FOR THE ARC WITH $P = Q = -1, \omega = 1.8$ AND 101 ITERATIONS WITH THE SOR METHOD

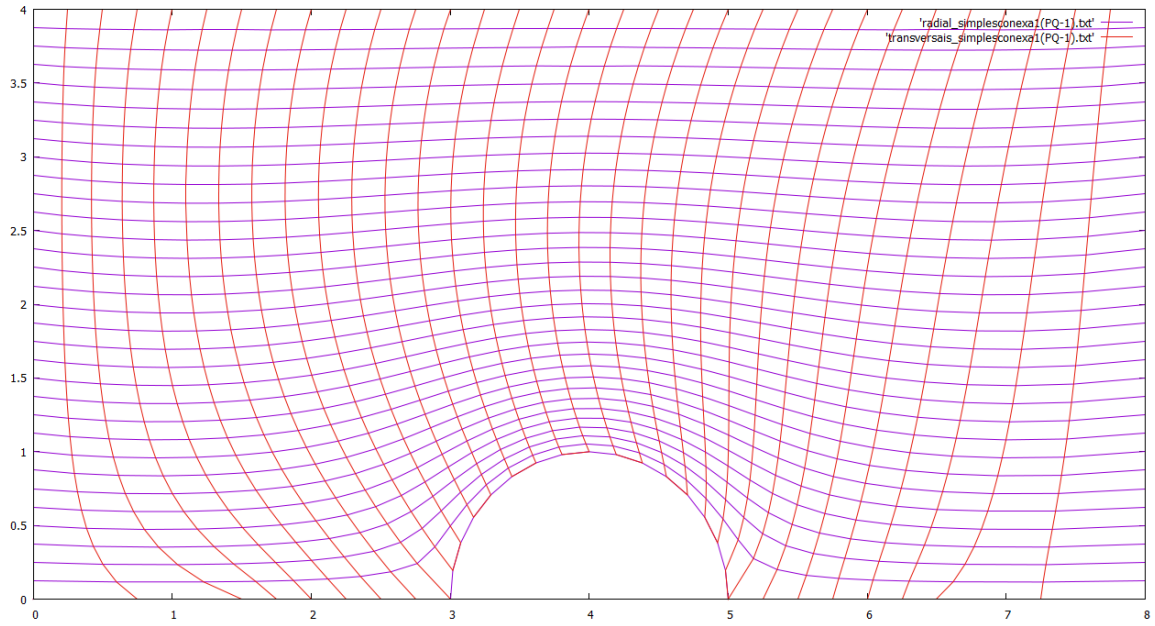

Source: Almeida (1997).

NACA0006

Figures 14 and 15 illustrate the meshes computationally generated from the points described in UIUC (2022).

FIGURE 14
MESH FOR NACA0006 (35 POINTS) WITH $P = Q = 0$ AND $R = 2, \omega = 1.6$ AND 121 ITERATIONS WITH THE SOR METHOD

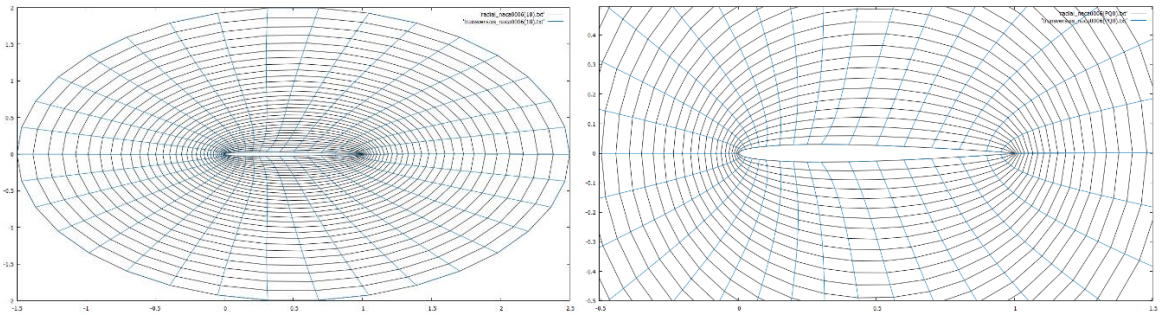

Source: Almeida (1997).

FIGURE 15
MESH FOR NACA0006 (35 POINTS) WITH $P = Q = -1$ AND $R = 2$, $\omega = 1.6$ AND 124 ITERATIONS WITH THE SOR METHOD

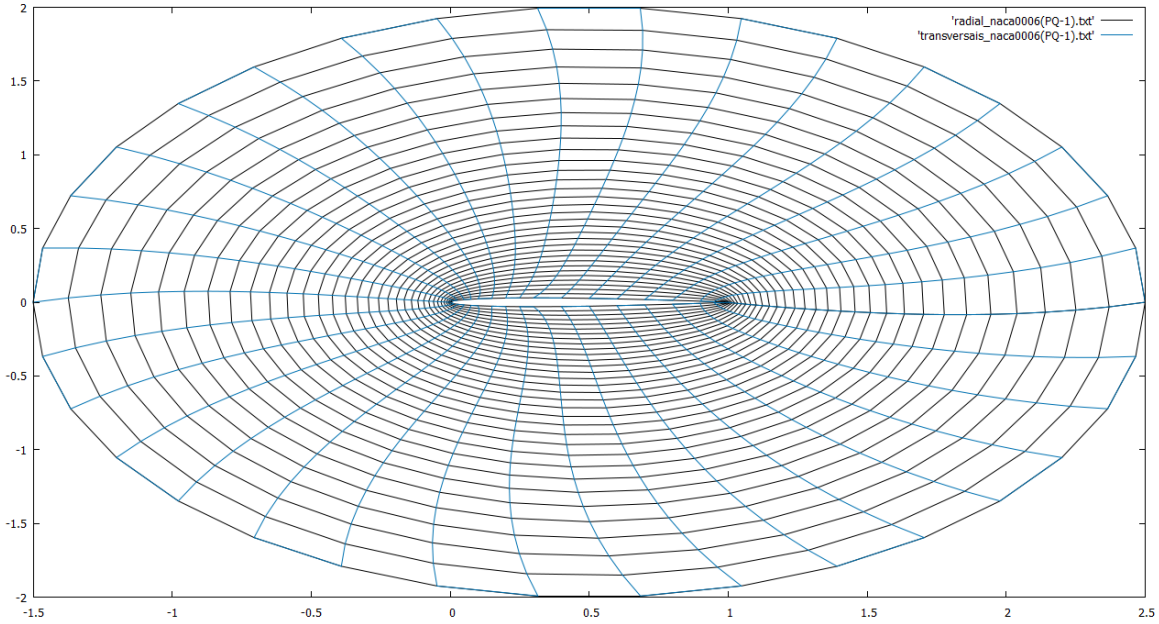

Source: Almeida (1997).

NACA2408

Figures 16 and 17 illustrate the meshes computationally generated from the points described in UIUC (2022).

FIGURE 16
MESH FOR NACA2408 (35 POINTS) WITH $P = Q = 0$ AND $R = 4.5$, $\omega = 1.7$ AND 157 ITERATIONS WITH THE SOR METHOD

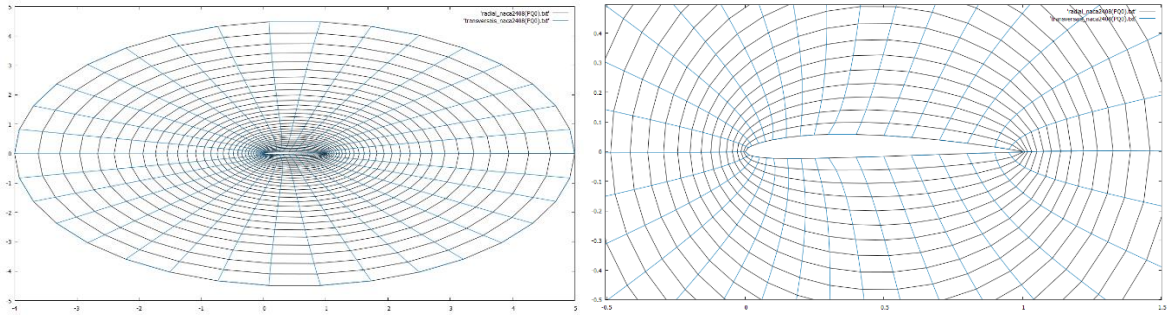

Source: Almeida (1997).

FIGURE 17
MESH FOR NACA2408 (35 POINTS) WITH $P = Q = 1$ AND $R = 4.5$, $\omega = 1.7$ AND 158 ITERATIONS WITH THE SOR METHOD

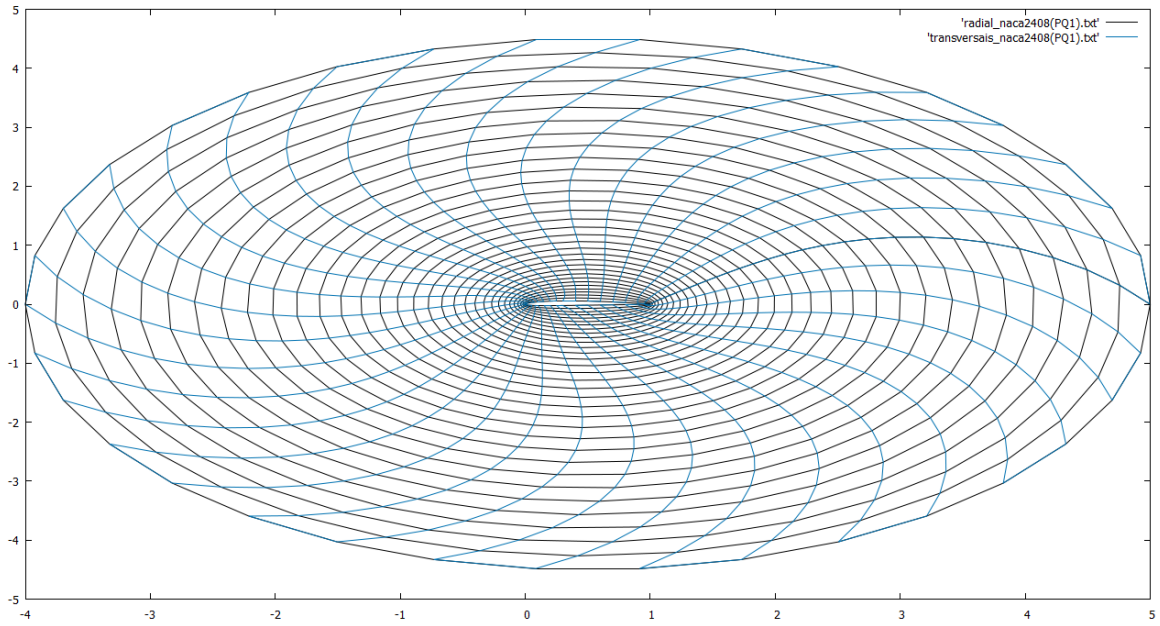

Source: Almeida (1997).

NACA23021

Figures 18 and 19 illustrate the meshes computationally generated from the points described in UIUC (2022).

FIGURE 18
MESH FOR NACA23021 (35 POINTS) WITH $P = Q = 0$ AND $R = 3$, $\omega = 1.8$ AND 98 ITERATIONS WITH THE SOR METHOD

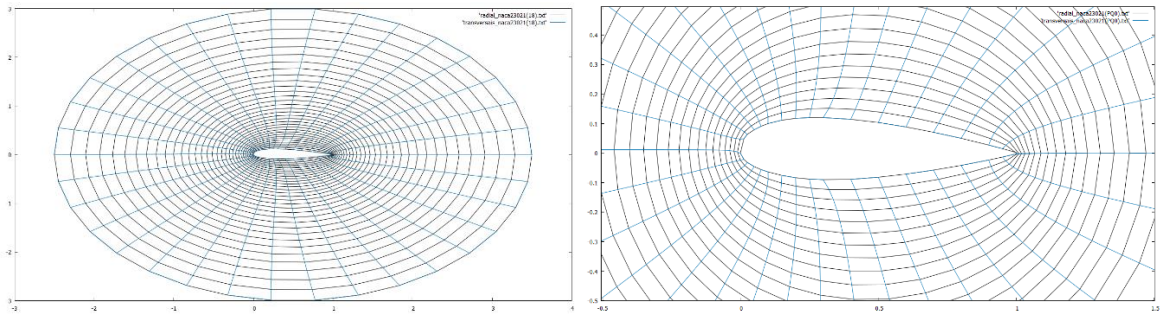

Source: Almeida (1997).

FIGURE 19
MESH FOR NACA23021 (35 POINTS) WITH $P = 1$, $Q = 0$ AND $R = 3$, $\omega = 1.8$ AND 110 ITERATIONS WITH THE SOR METHOD

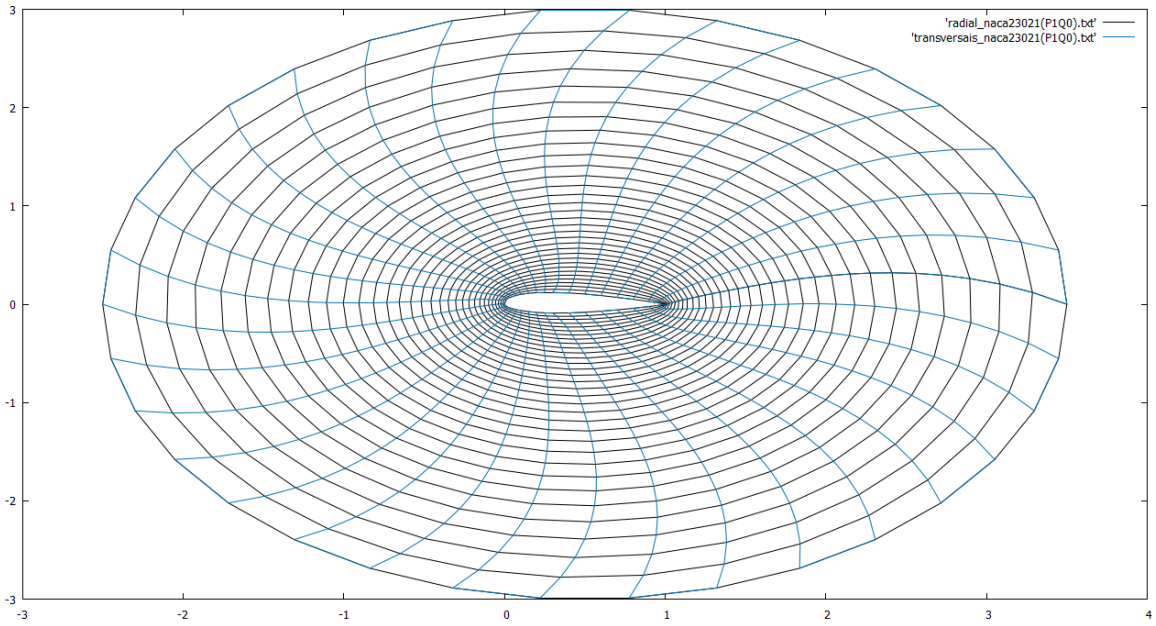

Source: Almeida (1997).

NACA25112

Figures 20 and 21 illustrate the meshes computationally generated from the points described in Airfoiltools (2022).

FIGURE 20
NACA25112 (121 POINTS) WITH $P = Q = 0$ AND $R = 8$, $\omega = 1.7$ AND 1334 ITERATIONS WITH THE SOR METHOD

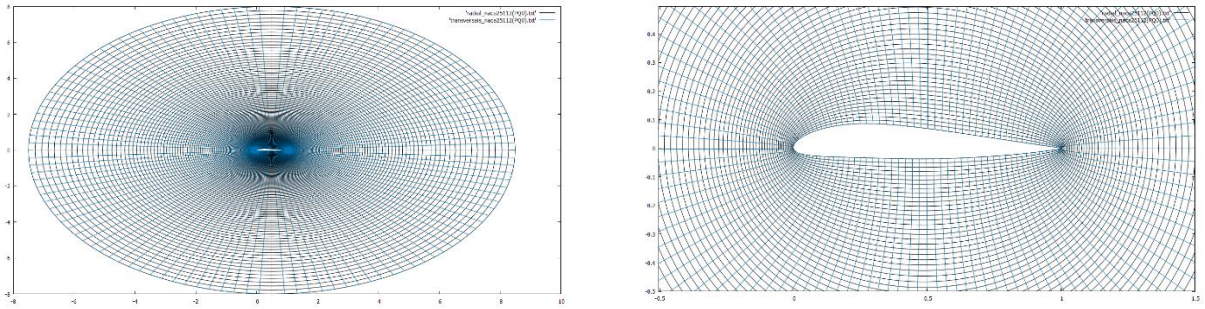

Source: Almeida (1997).

FIGURE 21
MESH FOR NACA25112 (121 POINTS) WITH $P = -1, Q = 1$ AND $R = 8, \omega = 1.7$ AND 1281 ITERATIONS WITH THE SOR METHOD

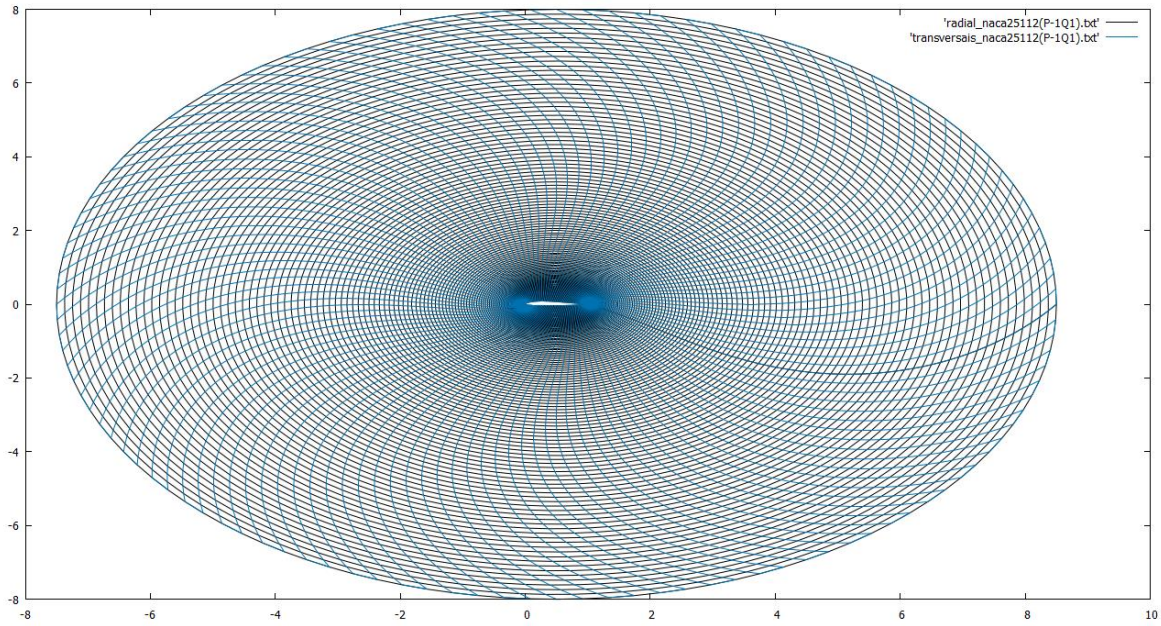

Source: Almeida (1997).

NACA747A415

Figures 22 and 23 illustrate the meshes computationally generated from the points described in UIUC (2022).

FIGURE 22
MESH FOR NACA747A415 (51 POINTS) WITH $P = Q = 0$ AND $R = 2, \omega = 1.5$ AND 240 ITERATIONS WITH THE SOR METHOD

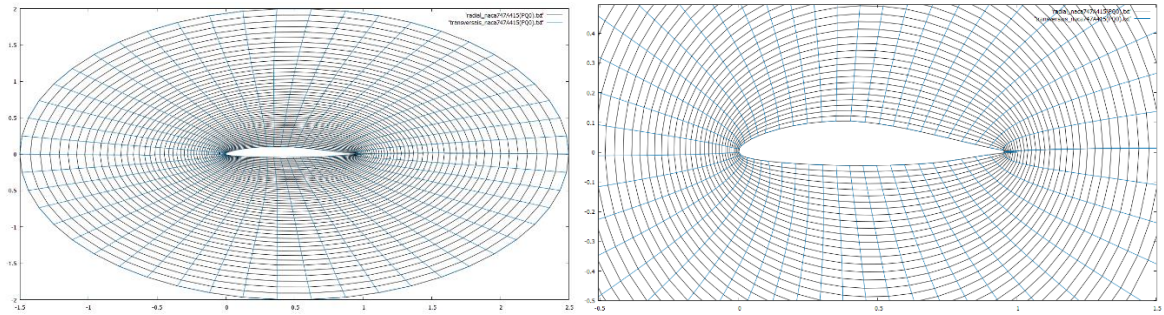

Source: Almeida (1997).

FIGURE 23
MESH FOR NACA747A415 (51 POINTS) WITH $P = Q = 10$ AND $R = 2, \omega = 1.5$ AND 246 ITERATIONS WITH THE SOR METHOD

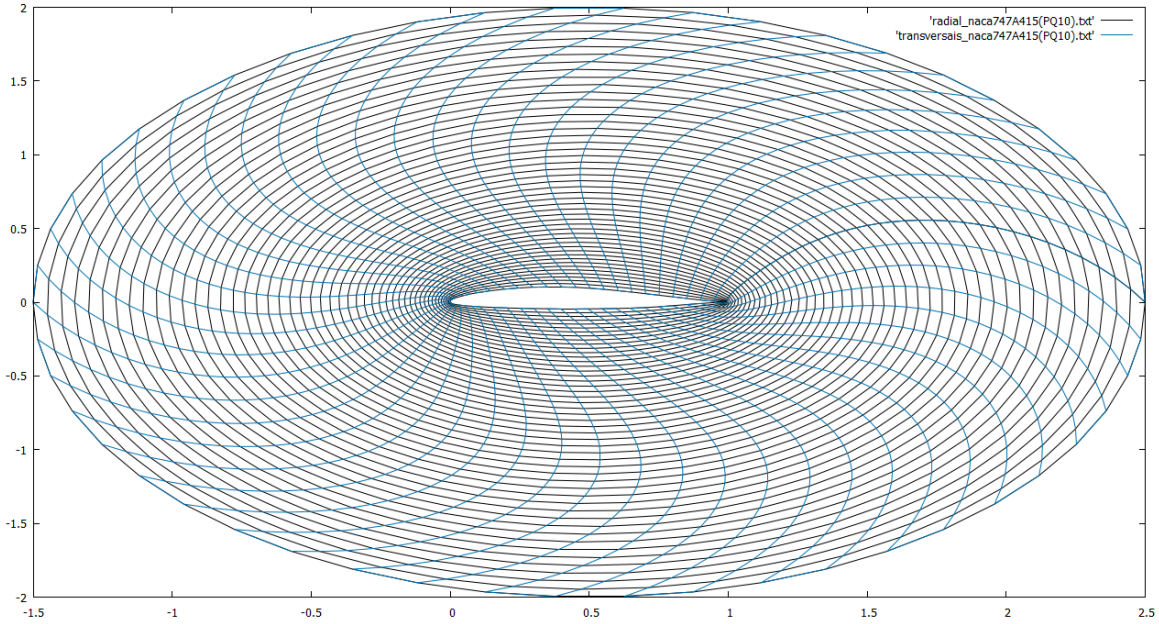

Source: Almeida (1997).

Orthogonal Meshes

The Thompson equations with spacing control (1)-(6) are reduced to

$$\frac{\partial^2 x}{\partial \xi^2} + \frac{\partial^2 x}{\partial \eta^2} = 0, \tag{17}$$

$$\frac{\partial^2 y}{\partial \xi^2} + \frac{\partial^2 y}{\partial \eta^2} = 0, \tag{18}$$

when considering $\alpha = \gamma = 1$, $\beta = 0$ e $P = Q = 0$.

Equations (17) and (18) can be employed to generate orthogonal meshes, since $\alpha = \gamma$ and $\beta = 0$ are orthogonality conditions (Thompson, 1985). Figure 24 illustrates orthogonal meshes generated from equations (17)-(18). However, there are other methods for generating orthogonal meshes, such as the Ryskin (Ryskin; Leal, 1983) and Brackbill (Brackbill; Saltzman, 1982) methods. In these methods, the Thompson equations (1)-(6) are used to generate the initial conditions.

FIGURE 24
ORTHOGONAL MESHES GENERATED FROM EQUATIONS (17)-(18): (A) DIFFUSER, WITH $\omega = 1.8$ AND 91 ITERATIONS WITH THE SOR METHOD; (B) ARC, WITH $\omega = 1.8$ AND 108 ITERATIONS WITH THE SOR METHOD

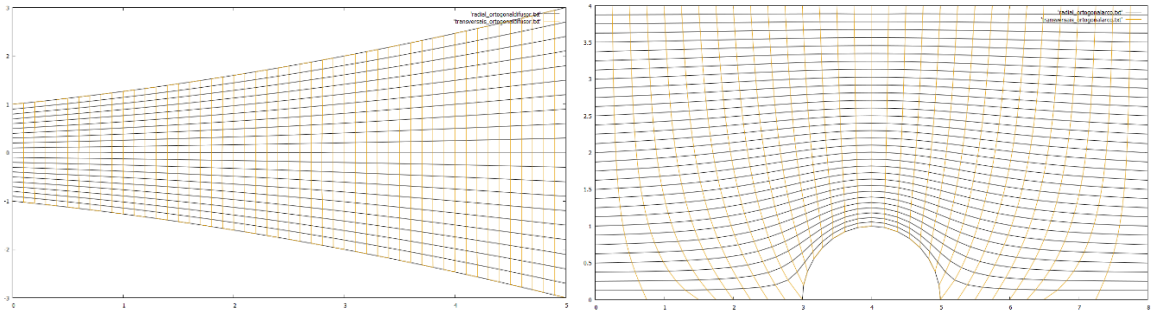

(a) (b)

Source: Almeida (1997).

CONCLUSION

In this paper, we present the Thompson equations with spacing factors P and Q and employ them to computationally generate two-dimensional structured meshes in simply and doubly connected geometries. In the doubly connected geometries, we use some wing profiles of an aircraft as the inner boundary.

To generate the meshes, we discretize the Thompson equations using second-order centered differences and solve the system of linear equations arising from the discretization using the SOR method. In this, we tested optimal values for the relaxation parameter ω. For the diffuser and the arc, the simply connected geometries adopted, we find that $\omega = 1.8$ establishes convergence with a smaller number of iterations, depending on the values adopted for P and Q. However, for NACAS, the doubly connected geometries adopted, we found that $1.5 \leq \omega \leq 1.8$ establishes convergence with a smaller number of iterations, depending on the values used for P and Q and also for the radius R of the circumference defining the radial boundary. One of the tests we performed for doubly connected geometries, NACA6409, illustrated in Figure 25, was divergent for all parameters P, Q, R and ω tested, thus evidencing that the combination of the SOR and finite difference methods is not always suitable for generating the meshes in any geometry.

FIGURE 25
AIRFOIL PROFILE: NACA6409

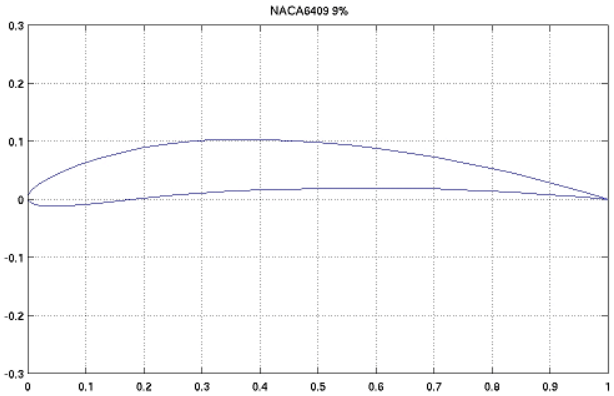

Source: UIUC (2022).

REFERENCES

Airfoil Tools. (2022). Retrieved January 26, 2022, from http://airfoiltools.com/index

Almeida, A.P.d. (2017). *Geração computacional de malhas bidimensionais estruturadas em torno da asa de uma aeronave*. 99 f. Monografia de Conclusão de Curso (Licenciatura em Matemática), Universidade Tecnológica Federal do Paraná (UTFPR), Curitiba, 2017. Retrieved from http://repositorio.roca.utfpr.edu.br/jspui/handle/1/9029

Almeida, A.P.De., & Nós, R.L. (2018). Geração de malhas computacionais estruturadas em torno da asa de uma aeronave. In: Congresso Nacional de Matemática Aplicada e Computacional, 37, 2017, São José dos Campos. *Proceeding Series of the Brazilian Society of Computational and Applied Mathematics*, *6*(1), 010148-1–010148-2. São Carlos: SBMAC.

Bloodshed. (2020). *Dev-C++ official website*. Retrieved from http://www.bloodshed.net/

Brackbill, J.U., & Saltzman, J.S. (1982). Adaptive zoning for singular problems in two dimensions. *Journal of Computational Physics*, *46*(3), 342–368.

Burden, R.L., & Faires, J.D. (1997). *Numerical analysis* (6th ed.). Pacific Grove: Brooks/Cole Publishing Company.

Figueiredo, D.G.d. (1997). *Análise de Fourier e equações diferenciais parciais*. Rio de Janeiro: IMPA.

Figueiredo, D.G.d., & Neves, A.F. (1997). *Equações diferenciais aplicadas*. Rio de Janeiro: IMPA.

Fortuna, A.de.O. (2000). *Técnicas computacionais para dinâmica dos fluidos: Conceitos básicos e aplicações*. São Paulo: Edusp.

Gnuplot. (2022). *Gnuplot homepage*. Retrieved from http://www.gnuplot.info

Iório, V. (1989). *EDP: Um curso de graduação*. Rio de Janeiro: IMPA.

Nós, R.L. (2007). *Simulações de escoamentos tridimensionais bifásicos empregando métodos adaptativos e modelos de campo de fase*. 179 f. Tese de Doutorado (Matemática Aplicada), Universidade de São Paulo (USP), São Paulo. Retrieved from https://teses.usp.br/teses/disponiveis/45/45132/tde-08052007-143200/pt-br.php

Paiva, A. (2013). *Geração de grid*. Retrieved from http://conteudo.icmc.usp.br/pessoas/apneto/cursos/2013/sme5827/aula04.pdf

Polina, S. *et al*. (1989). Geração de malhas para domínios bidimensionais simples e multiplamente conexos. In *Congresso Nacional de Matemática Aplicada e Computacional*. São José do Rio Preto.

Ryskin, G., & Leal, L.G. (1983). Orthogonal mapping. *Journal of Computational Physics*, *50*(1), 71-100.

Software de desenhos vetoriaislider do setor | Adobe Illustrator. (2021). Adobe. Retrieved January 27, 2022, from https://www.adobe.com/br/products/illustrator.html?promoid=KLXLT

Stanford. (n.d.). *The NACA airfoil series*. S. d. Retrieved from https://web.stanford.edu/~cantwell/AA200_Course_Material/The%20NACA%20airfoil%20series.pdf

Suckow, E. (2009). *Overview*. Retrieved January 27, 2022 https://history.nasa.gov/naca/overview.html

Thompson, J.F. (1985). *Numerical grid generation: Foundations and applications*. New York: Elsevier Science Publishing Co.

UIUC. (2022). *UIUC Airfoil coordinates database.* Retrieved from https://m-selig.ae.illinois.edu/ads/coord_database.html